AN INITIAL UNCERTAINTY ANALYSIS ON THE CRITICAL HEAT FLUX EVALUATION FOR A SMALL-SCALE PRESSURIZED NUCLEAR REACTOR USING THE COBRA CODE

J. P. Duarte, and J. R. C. Piqueira
University of São Paulo
Department of Telecommunications and Control Engineering, Polytechnic School
Av. Professor Luciano Gualberto, Travessa 3, 158, 05508-900, São Paulo, Brazil
julianapduarte@usp.br, piqueira@lac.usp.br

P. F. Frutuoso e Melo
Federal University of Rio de Janeiro
Graduate Program of Nuclear Engineering, COPPE
Av. Horácio Macedo 2030, Bloco G, Sala 206, Cidade Universitária
21941-914 Rio de Janeiro, RJ, Brazil
frutuoso@nuclear.ufrj.br

ABSTRACT

Uncertainty propagation was performed considering normal distributions for the input data for the critical heat flux (CHF) calculation, e.g., geometry, operation conditions, and thermal-hydraulic models (friction factor, void fraction, etc.). A test section for a small-scale design was analyzed using the COBRAIIIc/MIT-2 code and the EPRI correlation. The test section consists in a 3×3 bundle one meter high with a uniform power profile. The variation of all parameters generated a maximum variation of 33% on the CHF.

KEYWORDS
Critical heat flux, small-scale nuclear reactor, boiling crisis, uncertainty analysis

1. INTRODUCTION

The main goal of this work is to perform an uncertainty analysis on the critical heat flux (CHF) evaluation for a small-scale pressurized nuclear reactor (PWR). CHF or boiling crisis is one of the most important thermal-hydraulic phenomena in a PWR. It occurs in the heat transfer mechanism change from bubble to film transfer and leads to a huge wall temperature increase. The low mass flux, higher subcooling and a wider number of operating conditions for the small-scale reactor make the CHF conditions unusual compared to those of commercial PWRs. Therefore, a more detailed design of the experiments is needed in order to broadly understand CHF conditions for this type of reactor.

The CHF test section for a small-scale submarine reactor was previously analyzed [1] using a modified COBRAIIIc/MIT-2 code [2] and the EPRI correlation for CHF [3]. The test section consists in a 3×3 bundle one meter high with a uniform power profile. In this work, a new design of experiments is proposed considering pressure, mass flux and inlet subcoolant enthalpy and a Fortran 90 code was written to generate the COBRA inputs taking into account variable and model uncertainties, i.e., the uncertainty propagation was performed considering normal or uniform distributions for the input data for the CHF

calculation, such as geometry, operation conditions, and thermal-hydraulic models (friction factor, void fraction, etc.).

This paper is organized as follows. Section 2 presents the subchannel model used by COBRAIIIc/MIT-2 with the intention to clarify the parameters and models to be varied. Section 3 describes the results of the uncertainty analysis. The most significant variations in the CHF are shown by histograms. The conclusions are discussed in Section 4.

2. Subchannel analysis

The subchannel analysis is a widely used technique for studying the thermal-hydraulic behavior of nuclear reactor core. Its methodology consists of axially solving the mass, momentum and energy conservation equations considering two-phase flow and an interconnection between adjacent channels through cross-flow models. The control volume where these equations are solved numerically is usually defined between nuclear fuel rods.

The model used in COBRA IIIc/MIT-2, to be briefly discussed here, is based on the assumptions of a one-dimensional two-phase flow and separate phases. It is also assumed that the existing turbulent cross-flow between adjacent channels does not cause a net change in the flow redistribution.

Starting from the general continuity equation and since w_{ij} is the net flow rate of transverse flow from a channel j to a channel i for each axial unit length, the continuity equation can be expressed according to Eq. (1) [2]:

$$A_i \frac{\partial \rho_i}{\partial t} + \frac{\partial m_i}{\partial z} = -w_{ij} \tag{1}$$

The enthalpy variation in the control volume is given by the continuity equation, Eq. (2) [2]:

$$\frac{1}{u''}\frac{\partial h_i}{\partial t} + \frac{\partial h_i}{\partial z} = \frac{q'_i}{m_i} - \left(h_i - h_j\right)\frac{w'_{ij}}{m_i} - \left(t_i - t_j\right)\frac{c_{ij}}{m_i} + \left(h_i - h^*\right)\frac{w_{ij}}{m_i} \tag{2}$$

The left side of Eq. (2) gives the total enthalpy change in channel i. The first term on the right side of Eq. (2) is the ratio between the power and the flow rate of a subchannel and provides the enthalpy change rate if no turbulent mixing occurs. The second term considers the turbulent transport of enthalpy between all interconnected subchannels, where the turbulent thermal mixture w_{ij}' is defined by empirical correlations. The third term considers the lateral temperature gradient in the connection between two adjacent subchannels by a thermal conduction mixture coefficient c_{ij} [4]. Finally, the last term considers the thermal energy carried by the transverse diversion cross-flow.

At this point, it is important to highlight the difference between the two mechanisms that generate transverse mass flow. According to Refs. [4] and [5], the forced cross-flow, w_{ij} is associated with mass transfer between subchannels due to lateral pressure gradients caused by variations in geometry or non-uniform changes in fluid density. On the other hand, the turbulent cross-flow, w_{ij}', "is a floating mixing process with time caused by the turbulence of the fluid which surrounds the lateral mass transport of momentum and energy between adjacent subchannels" [4].

The conservation of the axial moment is given by Eq. 3 [2]. In addition to friction, acceleration and gravity components, this equation also displays the cross-flow components. The f_T coefficient is included

to help explain the imperfect analogy between the turbulent transport of enthalpy and momentum and is provided by the code user. k_i is a hydraulic resistance coefficient that depends on the characteristics of the local disturbance in the flow.

$$\frac{1}{A_i}\frac{\partial m_i}{\partial t} - 2u_i\frac{\partial p_i}{\partial t} + \frac{\partial p_i}{\partial z} = \left(\frac{m_i}{A_i}\right)^2\left[\frac{v_i f_i \phi}{2D_i} + \frac{k_i}{2\Delta z} + \frac{\partial\left(v_i/A_i\right)}{\partial z}\right] - \rho_i \cos\theta - \frac{f_T}{A_i}\left(u_i - u_j\right)w'_{ij} + \frac{1}{A_i}\left(2u_i - u^*\right)w_{ij} \tag{3}$$

Finally, we have the conservation of transverse momentum given by Eq. 4 [2],

$$\frac{\partial w_{ij}}{\partial t} + \frac{\partial\left(u_{ij} w_{ij}\right)}{\partial z} + \frac{s}{l}C_{ij} w_{ij} = \frac{s}{l}\left(p_i - p_j\right) \tag{4}$$

The first two terms represent the time and spatial acceleration of cross-flow. The *s/l* parameter represents the importance of the terms of transverse friction, C_{ij}, and pressure, p, versus the inertial terms and is provided by the code user.

2.1. Closure models

The single-phase model available in COBRAIIIc/MIT-2 model is based on the friction factor f_{iso} and Reynolds number according to Eq. (5):

$$f_{iso} = a\,\mathrm{Re}^b + c \tag{5}$$

where *a*, *b* and *c* are constants that depend on the specific channel roughness. The default values used for these coefficients are 0.184, -0.2 and 0.0, respectively, corresponding to the McAdams correlation whose validity is set for $10^4 < Re < 10^6$ [6].

This coefficient is corrected for heated walls by Eq. (6) [2],

$$f = f_{iso}\left\{1 + \frac{P_h}{P_w}\left[\left(\frac{\mu_{wall}}{\mu_{bulk}}\right)^{0.6} - 1\right]\right\} \tag{6}$$

where f_{iso} is evaluated by Eq. (5) and μ_{wall} is the viscosity evaluated at the wall temperature.

For the two-phase friction model, there are four options. The homogeneous model simply considers the two-phase friction multiplier, ϕ,, as in Eq. (7),

$$\begin{aligned} \phi &= 1.0 && x < 0 \\ \phi &= \frac{\rho_f}{\rho} && x > 0 \end{aligned} \tag{7}$$

The Armand model [7] for the two-phase friction multiplier, ϕ, is given by Eq. (8),

$$\begin{aligned}
&\phi = 1.0 && \alpha = 0 \\
&\phi = \frac{1-x}{(1-\alpha)^{1.42}} && 0.39 < \alpha \le 1.0 \\
&\phi = 0.478\frac{(1-x)^2}{(1-\alpha)^{2.2}} && 0.1 < \alpha \le 0.39 \\
&\phi = 1.730\frac{(1-x)^2}{(1-\alpha)^{1.64}} && 0.0 < \alpha \le 0.1
\end{aligned} \tag{8}$$

The other two options are the Baroczy model [2] and a polynomial function to be fitted to data.

Once the steam quality is determined, a model for the void fraction, α, should be used to calculate the vapor fraction of the control volume, Eq. (9),

$$\alpha = \frac{xv_g}{(1-x)Sv_f + xv_g} \tag{9}$$

The slip ratio S may be set equal to one (homogeneous model, where there is no slip between phases), or it may be estimated by the Smith correlation [8] (Eq. 10),

$$S = 0.4 + 0.6\left[\frac{0.4 + x\left(\frac{v_g}{v_f} - 0.4\right)}{0.4 + 0.6x}\right]^{1/2} \tag{10}$$

Smith points out that this correlation reproduces within 10% accuracy void fraction measurements taken in flows of water-steam and water-air in horizontal and vertical piping, at pressures of 0.1 to 14.5 MPa and vapor and air mass fractions from 0.01 to 0.5. Because of thermodynamic nonequilibrium, the equation is not recommended for qualities lower than 0.01 [4].

Another option available for the void fraction is the Armand-Massena correlation [9] (Eq. 11) or a polynomial model to be fitted by the code user,

$$\alpha = xv_g\frac{0{,}833 + 0{,}167x}{(1-x)v_f + xv_g} \tag{11}$$

This relationship applies to the pressure range between 1.8 and 20.7 MPa [4].

It is also necessary to choose a model for the turbulent cross-flow. The model used in this work is shown in Eq. 12 [2].

$$W' = aS_kG_k \tag{12}$$

The Beus model [10] for the mixture model was included in COBRAIIIc.

For the subcooled void calculation the code uses the Levy model [11], which calculates the actual quality as a function of the equilibrium quality and the flow quality. Table I summarizes the available models.

Table I. Options for closure models

Closure model	Options	Equation
Two-phase friction correlation	Homogeneous Theory Armand [7] Baroczy [2] Polynomial inequality	- (8) - -
Subcooled Void Indicator	No subcooled void Levy subcooled void correlation [11]	- -
Slip Ratio Indicator	Slip Ratio = 1 Armand Slip Ratio Correlation [9] Smith Slip Ratio Correlation [8] Slip ratio given by the user Void fraction as a polynomial in quality	- - (10) - -
Turbulent Mixing model	$W' = aS_k G_k$ Beus model [10]	(12) -
Cross-Flow Resistance Coefficient	k (default is 0.5)	(3)
Turbulent Momentum Factor	f_t (default is 0.0)	(3)
Transverse Momentum Factor	s/l (default is 0.5)	(4)
Inclination of channel to vertical	θ (degrees)	(3)

3. RESULTS AND DISCUSSION

The uncertainty in any analysis can be divided in three types: parameter, modeling and completeness. The first one includes the input data error, as the geometry uncertainty due to fabrication and correlation uncertainties that comes from experimental data. This type of uncertainty can be evaluated using a Monte Carlo method and combing all inputs values (using their probability distributions) to find the output range.

The second type of uncertainty includes the mathematical or numerical approximations that are made for convenience and the model validation range. Finally, the last type is related to our current state of knowledge about the subject and to the sufficient depth that have been used in the analysis.

This paper focuses on the first kind of uncertainty, which is subdivided into three types related to geometry, model choices, and operating conditions. The objective is to analyze the influence of these factors in the simulation through the COBRA computer code. Although the geometry and operating conditions are intrinsically experimental uncertainties one can, with a bit more computational effort, predict the influence of these variations. The geometry of the experimental design may vary due to limitations in the manufacturing process and due to thermal expansion.

Table II shows the performed experimental design and the value of the average critical heat flux in kW/m^2 for each inlet subcooling, pressure and mass flux conditions (in parentheses is the number associated with the experimental conditions, ranging from 1 to 100) . The average value of the critical heat flux is defined as the total power divided by the rod heat transfer area. We considered for the simulation the Armand model [7] to calculate the two-phase friction coefficient, the Smith model [8] for the void fraction, the Beus model [10] for turbulent mixing and the default values shown in Table I for the f_T, k and s/l coefficients. For all the simulations, we used the McAdams model for the single-phase friction coefficient and the EPRI correlation for the critical heat flux [3].

Table II. Average critical heat flux

CHF (kW/m^2)		**Inlet subcoolant (kJ/kg)**					**Pressure (MPa)**
		60	**220**	**380**	**540**	**700**	
Mass flux ($kg/m^2.s$)	**203**	557 (1)	640 (2)	731 (3)	820 (4)	915 (5)	**12.0**
		496 (6)	570 (7)	651 (8)	735 (9)	823 (10)	**13.1**
		429 (11)	494 (12)	567 (13)	646 (14)	726 (15)	**14.3**
		364 (16)	421 (17)	488 (18)	548 (19)	562 (20)	**15.5**
	381	713 (21)	830 (22)	964 (23)	1110 (24)	1256 (25)	**12.0**
		638 (26)	745 (27)	872 (28)	1008 (29)	1143 (30)	**13.1**
		561 (31)	657 (32)	777 (33)	906 (34)	1027 (35)	**14.3**
		487 (36)	577 (37)	691 (38)	809 (39)	914 (40)	**15.5**
	627	863 (41)	1025 (42)	1205 (43)	1388 (44)	1565 (45)	**12.0**
		779 (46)	931 (47)	1101 (48)	1270 (49)	1433 (50)	**13.1**
		696 (51)	836 (52)	996 (53)	1151 (54)	1297 (55)	**14.3**
		617 (56)	750 (57)	898 (58)	1040 (59)	1180 (60)	**15.5**
	764	930 (61)	1117 (62)	1317 (63)	1516 (64)	1712 (65)	**12.0**
		844 (66)	1020 (67)	1209 (68)	1395 (69)	1574 (70)	**13.1**
		759 (71)	922 (72)	1101 (73)	1272 (74)	1440 (75)	**14.3**
		679 (76)	835 (77)	1001 (78)	1159 (79)	1323 (80)	**15.5**
	1117	1073 (81)	1321 (82)	1570 (83)	1817 (84)	2065 (85)	**12.0**
		985 (86)	1221 (87)	1458 (88)	1692 (89)	1931 (90)	**13.1**
		899 (91)	1121 (92)	1349 (93)	1572 (94)	1803 (95)	**14.3**
		818 (96)	1033 (97)	1249 (98)	1468 (99)	1692 (100)	**15.5**

The local critical heat flux is shown by response surfaces in Figure 1 as a function of the independent variables coded from -1 to +1, where -1 is the lowest value and the highest value is +1. The critical heat flux increases with the increase of subcooling and the increase of mass flux and decreases with increasing pressure, as set forth in literature [12].

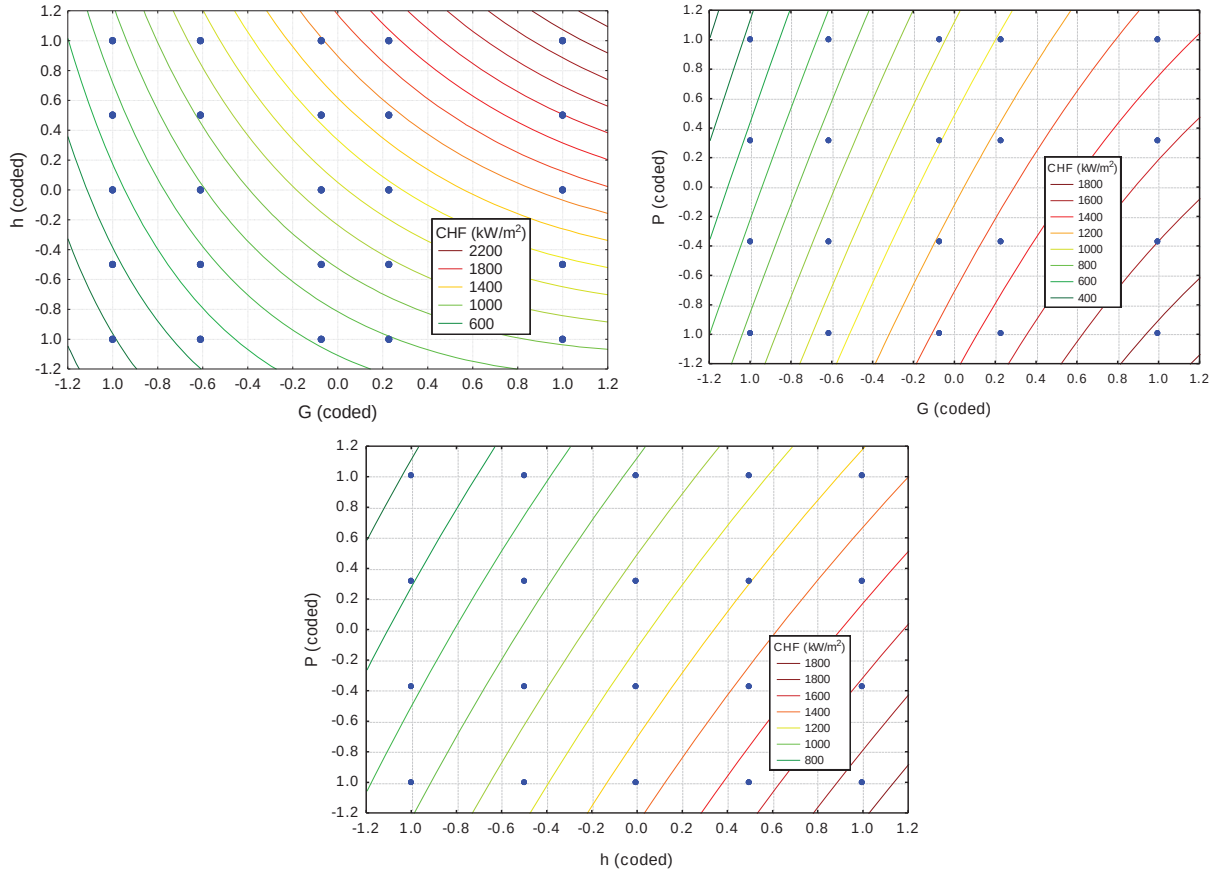

Figure 1. Local critical heat flux response surface.

Table III summarizes the sensitivity analyzes performed for each parameter. The type of change performed for each parameter is indicated in the third column, where $N(\mu,\sigma)$ represents a normal distribution with mean μ and standard deviation σ and $U(a,b)$ is a uniform distribution between the values a and b. The results of these variations in the maximum and minimum average critical heat flux is shown in columns four and five, respectively. The largest variation observed for the simulated hundred points is shown in the last column with the experiment number in parentheses. The variation was calculated by the difference between the highest and the lowest CHF due to the variation of each parameter divided by the reference value in Table I.

The number of simulation cases for each of the hundred conditions in experimental design is also shown in Table I. The computational time to simulate the proposed 100 operating conditions is approximately 6 seconds, totaling around 10 minutes to simulate 100 × 100 simulations. Table III and Figures 2-8 display the results of 110,200 simulations for a total time of less than 2 hours.

The variation in geometry of the rod diameter, pitch and gap (distance between the center of the lateral rod and the bundle wall), where a standard deviation of 1% from the reference value was considered, generated a maximum variation of 8% in the CHF for the first experiment (with lower pressure, mass flux and inlet subcoolant). Figure 2 shows the CHF for this case.

Among the options of the COBRA parameters and models, the only one that was significant for the conditions considered was the turbulent mixing model. The Beus model generated a lower critical heat flux, while the model of Eq. (12) increased the CHF with increasing coefficient a. Figure 3 shows this

influence for the case # 85 for which we obtained the highest CHF (lower inlet subcooling, greater mass flux and lower pressure).

The only parameter that showed a little influence on the CHF value was the ratio *s/l* of Eq. (4). The maximum variation occurred in case #20 for the ratio *s/l* equal to 0.0352 (Fig. 4). The rod bundle angle change from 0° (vertical) to 90° (horizontal position) does not influence the CHF, showing a possible limitation of COBRA. However, there is a suspicion that the inclination can influence the results, since the cross-flow models may no longer be valid. Thus, the use of computational fluid dynamics analysis is recommended in this case.

Table III. Sensitivity analysis

Parameter	# Cases	Variation*	$CHF_{avg,max}$	$CHF_{avg,min}$	Maximum variation (case #)
Geometry (D_{rod}, Pitch, gap)	98	N(μ, μ×0.01)	2121.1 (+3%)	353.6 (-3%)	8% (1)
Turbulent mixing model	100	N(0.02, 0.01)	2388.0 (+16%)	361.8 (-1%)	21% (1)
Two phase friction model	2	Armand Baroczy	2065.9 (0%)	364.0 (0%)	0%
Void model	2	Armand Smith	2065.9 (0%)	364.0 (0%)	0%
k	100	N(0.5, 1.0)	2065.9 (0%)	364.0 (0%)	0%
f_t	100	N(0.0, 0.3)	2065.9 (0%)	364.0 (0%)	0%
s/l	100	N(0.5, 1.0)	2068.1 (0%)	359.6 (-1%)	3% (20)
Theta	100	U(0, 90)	2065.9 (0%)	364.0 (0%)	0%
Pressure	100	N(μ, μ×0.01)	2083.8 (1%)	343.9 (-6%)	18% (19)
Temperature**	100	N(μ, μ×0.01)	2099.4 (2%)	342.9 (-6%)	27% (96)
Mass flux	100	N(μ, μ×0.01)	2088.7 (1%)	359.3 (-1%)	4% (19)
All parameters	200	--	2458.1 (19%)	345.7 (-5%)	33% (96)

*$N(\mu, \sigma)$ represents a normal distribution of mean μ and standard deviation σ, where the mean was the reference value in the experimental design.

**Standard deviation of 1% was considered for values in Fahrenheit degrees, resulting in slight higher variation in Celsius degrees.

Assuming a standard deviation of 1% of the reference values of pressure, temperature and mass flux, we obtained a CHF variation of up to 18%, 27% and 4%, respectively, as shown in Figures 5-7. Finally, considering the variation of all parameters of Table III the distribution obtained for the CHF is presented in Figure 8 with a 33% change in case # 96 (greater mass flux, higher pressure and lower subcooling).

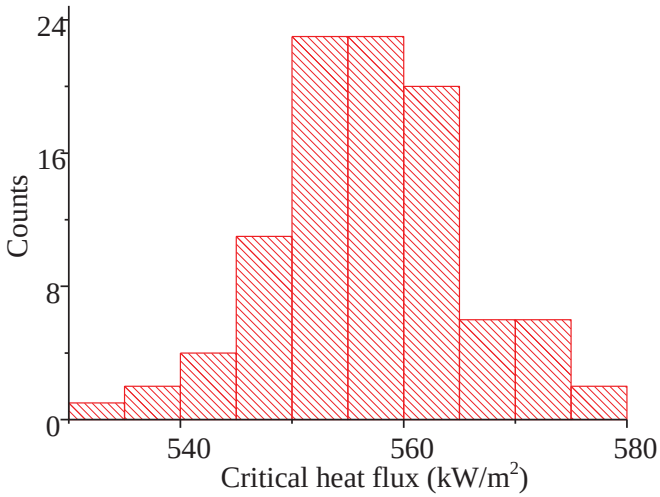

Figure 2. Average critical heat flux variation due to the geometry variation for case #1

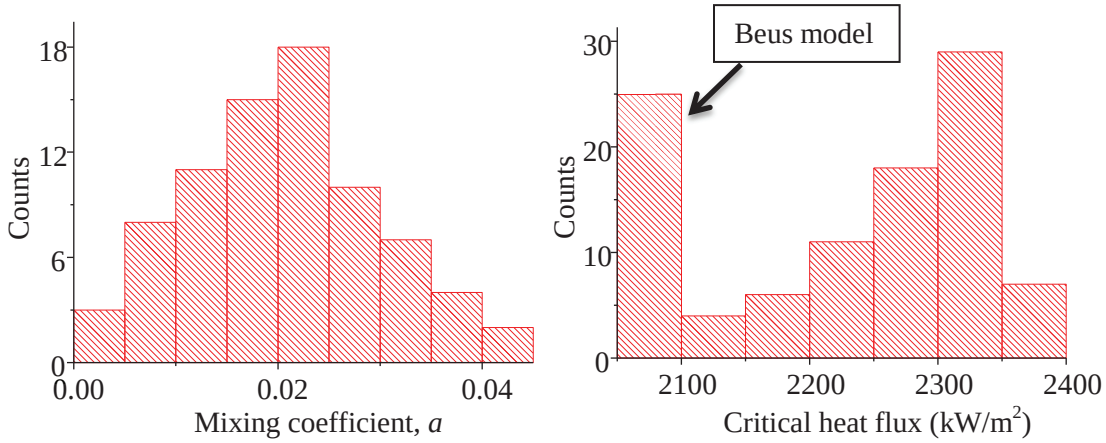

Figure 3. Average critical heat flux variation due to the turbulent mixing model for case #85. At the left, the input mixing coefficient and at the right, the output CHF

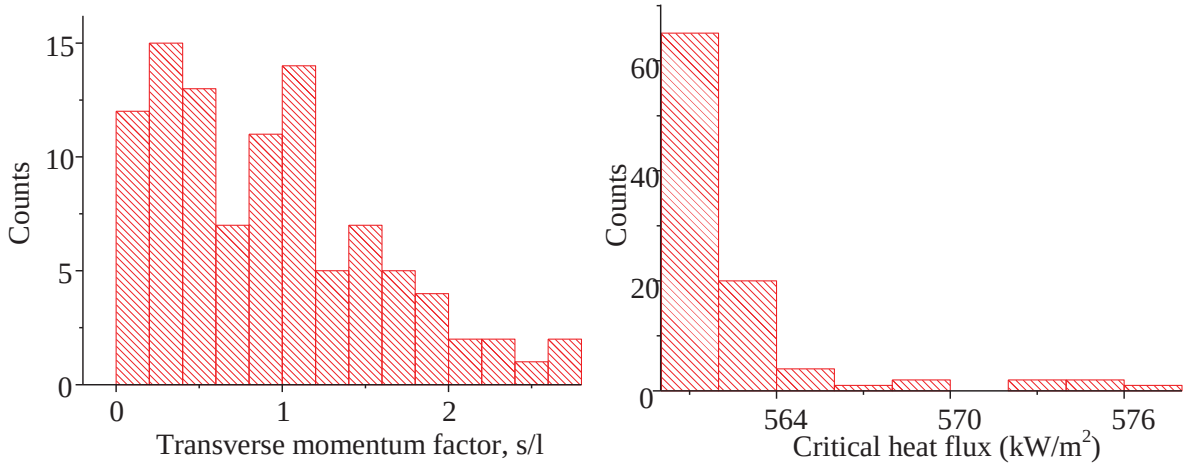

Figure 4. Average critical heat flux variation due to the transverse momentum factor for case #20. At the left, the input variation and at the right, the output CHF

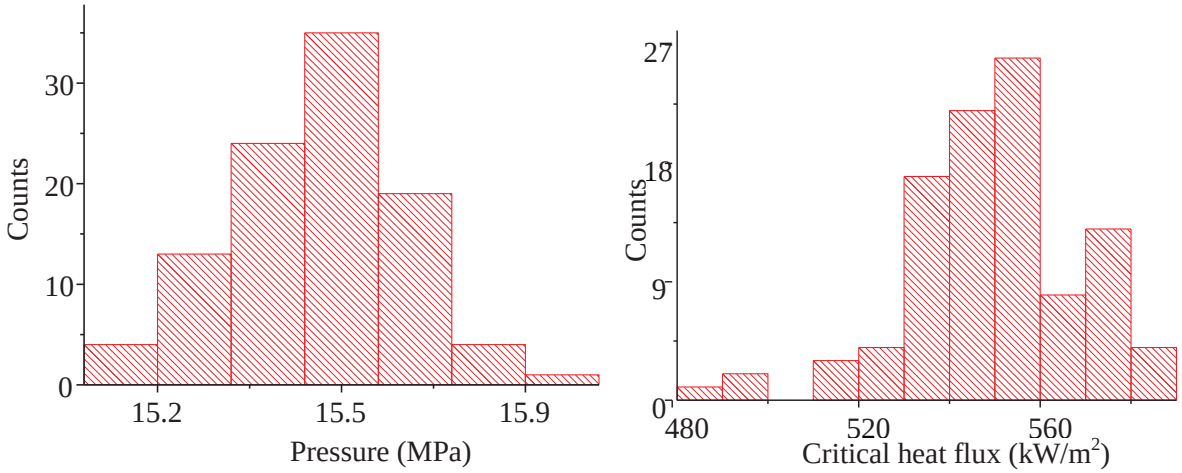

Figure 5. Average critical heat flux due to 1% variation of pressure for case #19. At the left, the input pressure distribution and at the right, the output CHF

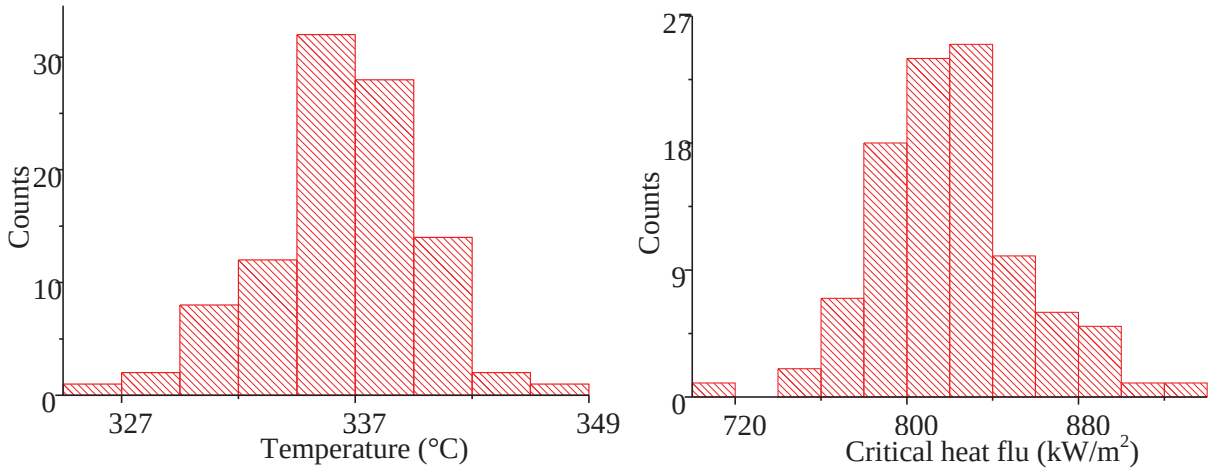

Figure 6. Average critical heat flux due to 1% variation of temperature for the case #96. At the left the input temperature distribution and at the right the output CHF

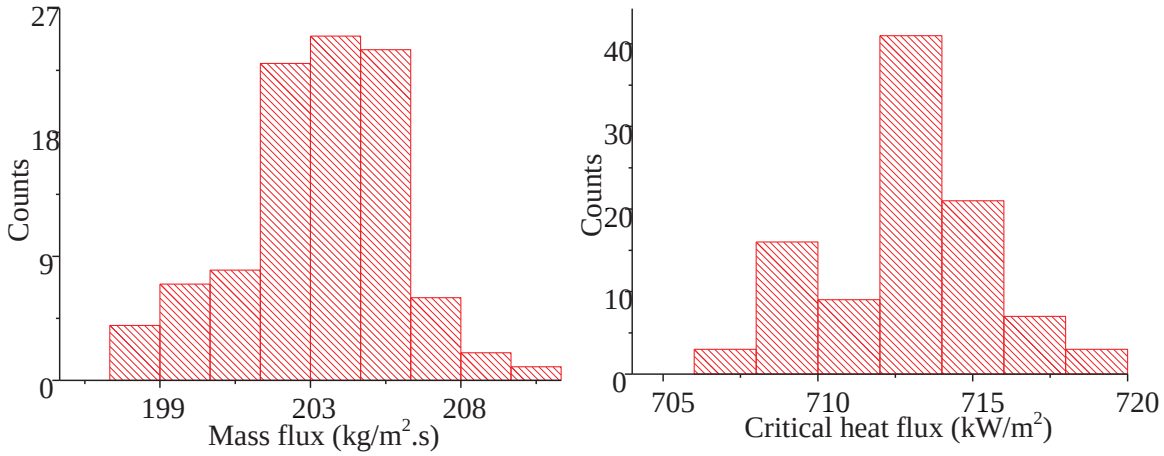

Figure 7. Average critical heat flux due to 1% variation of mass flux for case #19. At the left, the input mass flux distribution and at the right, the output CHF

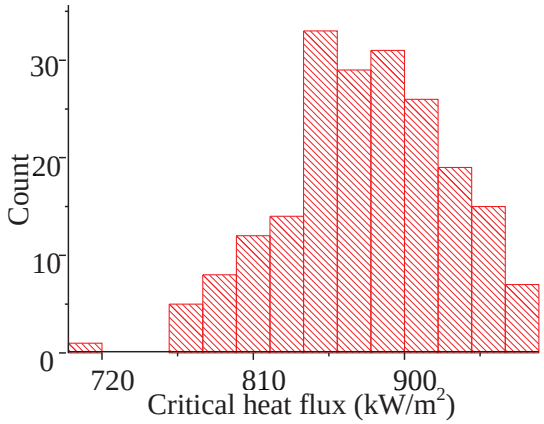

Figure 8. Average critical heat flux variation for all parameter variations for case #96

4. CONCLUSIONS

Test sections were simulated to analyze the critical heat flux using the COBRAIIIc/MIT-2 for the conditions of a small PWR. The EPRI correlation for the CHF was chosen for covering the experimental conditions and an initial uncertainty evaluation was performed.

This work showed that with a little more computational effort it is possible to predict the simulation results considering uncertainty sources. Three types of uncertainties were analyzed: changes in geometry resulted in a change of up to 8% in the CHF; the model selection affected up to 18%; and a 1% change in the operating conditions resulted in a variation of up to 27% of the predicted value for the CHF.

The importance of using this type of analysis is not only to predict the simulation variations, but also to identify possible code limitations.

NOMENCLATURE

A_i – flow area;
c_{ij} – mixture coefficient of thermal conduction;
C_{ij} – transverse friction coefficient;
D_i – equivalent hydraulic diameter for channel i;
f – corrected single-phase friction coefficient;
f_{iso} – single-phase friction coefficient;
f_T – turbulent momentum factor;
G_k – mass flux;
h – enthalpy;
k_i – hydraulic resistance coefficient;
m_i – mass flow;
p – pressure in channel i;
P_h – heated perimeter;
P_w – wetted perimeter;
q_i' – power for unit lenght;
Re – Reynolds number;
S – slip ratio between vapor and liquid phases;
s/l – transverse momentum factor;

S_k – gap width;
t – time;
$t_{i,j}$ – channel temperature;
u'' – effective velocity for energy transport;
u_i – transport velocity for axial momentum;
v_f – liquid specific volume;
v_g – vapor specific volume;
v_i – effective specific volume for momentum transport;
w_{ij} – net rate of cross-flow from channel j to channel i;
w_{ij}' – turbulent thermal mixture;
x – quality;
z – axial position;
α – volumetric void fraction;
ϕ – two-phase friction multiplier;
μ_{bulk} – viscosity at the bulk temperature;
μ_{wall} – viscosity at the wall temperature;
θ – bundle inclination angle;
ρ – fluid density.
ρ_f – liquid density.

ACKNOWLEDGMENTS

Thanks go to the University of São Paulo and to São Paulo Research Foundation for their invaluable support.

REFERENCES

1. J. P. Duarte, M. A. Veloso, M. E. S. Taqueda, and J. R. C. Piqueira, "A Design of Experiments for Critical Heat Flux Evaluation of a Small-Scale Pressurized Water Reactor", *Nuclear Engineering and Design*, submitted for publication (2015).
2. J. W. Jackson, and N. E. Todreas, "COBRA IIIc/MIT-2: A Digital Computer Program for Steady State and Transient Thermal-Hydraulic Analysis of Rod Bundle Nuclear Fuel Elements". MIT-EL 81-018. Cambridge, MA: Massachusetts Institute of Technology (1981).
3. EPRI, "Parametric Study of CHF Data, Volume 1: Compilation of Rod", NP-2609, Final Report, January, New York, US (1982).
4. M. A. Veloso, "Computational Simulation of Thermal-hydraulic Transients Considering many Circuits and Pumps". PhD thesis, Chemical Engineering College, State University of Campinas, (2003) (in Portuguese).
5. N. E. Todreas, and M. S. Kazimi, "Nuclear System II – Elements of Thermal Hydraulic Design". New York, NY: Hemisphere Publishing Corporation. 506 p (1990).
6. N. E. Todreas, and M. S. Kazimi, "Nuclear Systems, Volume 1 - Thermal Hydraulic Fundamentals", 2nd ed., CRC Press, US (2012).
7. A. A. Armand, "The resistance during the movement of a two-phase system in horizontal pipes", AERE Trans 828. Translated by Beak from article published in the Soviet journal *Izvestiya Vsesoyuznogo Teplotekhnicheskogo*, n. 1, p. 16-23, 1946. Harwell, Berkshire,UK: Atomic Energy Research Establishment, (1959).
8. S. L. Smith, "Void fractions in two-phase flow: a correlation based upon an equal velocity head model". *Proc. Instn. Mech. Engrs*., v. 184, pt. 1, n. 36, p. 647-664 (1969-70).

9. W. A. Massena, “Steam-Water Pressure Drop Critical Discharge Flow – A Digital Computer Program”. HW–65706. Richland, WA: Hanford Atomic Products Operation (1960).
10. S. G. Beus, “A Two-Phase Turbulent Mixing Model for Flow in Rod Bundles”. WAPD-T-2438. Pittsburgh, PA: Bettis Atomic Power Laboratory (1971).
11. S. Levy. “Forced Convection Subcooled Boiling-Prediction of Vapor Volumetric Fraction”, GEAP-5157. General Electric Co., Atomic Power Equipment Dept., San Jose, California (April 1966).
12. L. S. Tong and Y. S. Tang, “Boiling Heat Transfer and Two-Phase Flow”, 2nd ed., Taylor & Francis, US (1997).